Analytical solution of low Reynolds number slip flow past a sphere

R. W. Barber and D. R. Emerson

Centre for Microfluidics,
Department of Computational Science and Engineering,
CLRC Daresbury Laboratory,
Daresbury,
Warrington,
WA4 4AD.

Abstract

An analytical solution is derived for predicting low Reynolds number rarefied gas flow past an unconfined sphere. In Stokes' original analysis of creeping flow past a sphere, a continuum flow hypothesis was implemented and no-slip boundary conditions were utilised on the surface. However, when the size of the sphere approaches the mean free path of the gas molecules, Stokes' continuum hypothesis breaks down and it is then important to account for rarefaction effects. In the present work, Stokes' solution has been extended for use in the *slip-flow* regime which is valid for Knudsen numbers, $Kn \leq 0.1$. The total drag on the sphere is shown to be equivalent to Stokes' solution for continuum flows multiplied by a rarefaction coefficient which is dependent upon the Knudsen number.

Applying the slip-flow technique to the estimation of the terminal velocity of a microsphere shows that rarefaction effects increase the predicted settling speed. This result is confirmed by comparing the analytical solution with the experimental terminal velocities obtained in Millikan's landmark oil drop experiment. An additional validation study has also been conducted which compares the analytical drag formulae against numerical predictions from a finite-volume Navier-Stokes solver.

1 Introduction

The rapid progress in fabricating and utilising Micro Electro Mechanical Systems (MEMS) during the last decade has led to considerable research in the unconventional physics involved in the manufacture and operation of miniaturised devices [1,2,3]. Such devices have been widely used in instrumentation, micro-reactors, actuators and "lab-on-a-chip" bio-chemical sensors. Although successful fluid manipulation is often crucial to the overall operation of a MEMS device, microfluidic systems frequently rely on trial-and-error design techniques.

One of the main difficulties in trying to predict fluid transport in micron-sized devices lies in the fact that the continuum flow assumption implemented in conventional fluid dynamics breaks down because of the very small length scales involved. For example, the mean free path of air molecules at standard temperature and pressure is approximately 70 nm (see Appendix). Consequently, the ratio of the mean free path of the molecules to the characteristic dimensions of a MEMS device can be appreciable. This ratio is referred to as the Knudsen number and as it increases, the momentum transfer starts to be affected by the discrete molecular composition of the fluid; in other words the gas begins to exhibit non-continuum flow effects. Until recently, non-continuum flows were only encountered in low-density (rarefied gas) applications such as vacuum or space-vehicle technology. One of the main distinctions between conventional rarefied gas dynamics and microfluidic processes lies in the fact that rarefaction effects in MEMS take place at normal operating pressures. The small lengths and fluid velocities employed in MEMS also lead to extremely low Reynolds numbers. Consequently, the analysis of gaseous transport in microfluidic devices often involves the intriguing combination of rarefied gas dynamics *and* ultra low Reynolds number (creeping) flows.

Increasing research emphasis has been directed towards the extension of existing Navier-Stokes codes to include rarefaction effects [4,5,6]. Additionally, analytical solutions have been developed for a number of simple device geometries including long straight microchannels [7-13]. The present study describes an extension of Stokes' analytical solution [14] for creeping flow past a sphere which takes into account rarefaction (non-continuum) effects. The analysis follows the slip-flow methodology originally proposed by Basset [15]. Specifically the present analysis has been directed towards the estimation of the individual drag force components experienced by a microsphere subjected to unconfined low Reynolds number gas flow. The analytical method may have important implications in estimating the terminal velocity and sedimentation of micron-sized particulates, as well as providing an analytical solution to validate micro-scale hydrodynamic codes.

2 Governing hydrodynamic equations of creeping flow

The Navier-Stokes equations governing the flow of an incompressible, Newtonian fluid of constant viscosity can be written as

$$\nabla \cdot \vec{u} = 0 \tag{1}$$

and

$$\rho\frac{D\vec{u}}{Dt}\equiv\rho\frac{\partial\vec{u}}{\partial t}+\rho\,\vec{u}\cdot\nabla\vec{u}=-\nabla p+\mu\nabla^2\vec{u} \tag{2}$$

where $\vec{u}$ is the velocity vector, *D/Dt* is the total derivative, *p* is the pressure, ρ is the fluid density and μ is the coefficient of dynamic viscosity. Consider a flow having a characteristic length L_c and characteristic velocity U_c. The Navier-Stokes equations can be non-dimensionalised with respect to the following dimensionless variables:

$$\vec{u}^*=\frac{\vec{u}}{U_c}\qquad t^*=\frac{t\,U_c}{L_c}\qquad \nabla^*=L_c\nabla\qquad \nabla^{2*}=L_c^2\nabla^2\qquad p^*=\frac{p}{(\mu U_c/L_c)} \tag{3}$$

Substitution into the continuity equation (1) yields

$$\frac{U_c}{L_c}\nabla^*\cdot\vec{u}^*=0\qquad\Rightarrow\qquad\nabla^*\cdot\vec{u}^*=0 \tag{4}$$

whilst substitution into (2) gives

$$\frac{\rho U_c^2}{L_c}\frac{\partial\vec{u}^*}{\partial t^*}+\frac{\rho U_c^2}{L_c}\vec{u}^*\cdot\nabla^*\vec{u}^*=-\frac{\mu U_c}{L_c^2}\nabla^* p^*+\frac{\mu U_c}{L_c^2}\nabla^{2*}\vec{u}^* \tag{5}$$

which can be rewritten as

$$\mathrm{Re}\left\{\frac{\partial\vec{u}^*}{\partial t^*}+\vec{u}^*\cdot\nabla^*\vec{u}^*\right\}=-\nabla^* p^*+\nabla^{2*}\vec{u}^* \tag{6}$$

where $Re=\rho U_c L_c/\mu$. Thus for small Reynolds numbers, typically *Re* < 1, the inertia terms on the left-hand side of the momentum equation (6) can be neglected, giving *Stokes' equation*:

$$\nabla p=\mu\nabla^2\vec{u} \tag{7}$$

represented here in terms of the original variables. By taking the curl and then the gradient of eqn. (7), it can be shown that both the vorticity, $\vec{\omega}$ and pressure satisfy Laplace's equation:

$$\nabla^2\vec{\omega}=0 \tag{8}$$

and

$$\nabla^2 p=0 \tag{9}$$

In planar two-dimensional flows the vorticity vector $\vec{\omega}$ has a single scalar component which can be found by introducing the streamfunction, ψ. Specifically, the vorticity is related to the streamfunction by:

$$\vec{\omega} = -\nabla^2 \psi \tag{10}$$

and hence eqn. (8) can be rewritten as a biharmonic equation:

$$\nabla^4 \psi = 0 \tag{11}$$

3 Slip flow around a solid microsphere

Consider a stationary solid microsphere of radius, *a* in an unbounded incompressible Newtonian fluid of density, ρ and viscosity, μ as shown in Figure 1. The flow infinitely far from the sphere is of uniform speed U_∞. It is convenient to use spherical polar co-ordinates (r, θ, α) to analyse the problem, with the origin at the centre of the sphere and $\theta = 0$ aligned in the direction of U_∞. Since the flow field is axisymmetric, $\vec{u}$ and *p* are independent of α. In addition, as the approach flow is free from swirl, the entire flow domain will be free from swirl and consequently $\vec{u}$ has no component in the α-direction. It is therefore possible to analyse the problem as a planar two-dimensional flow and work in terms of Stokes' streamfunction, ψ:

$$u_r = \frac{1}{r^2 \sin\theta} \frac{\partial \psi}{\partial \theta} \qquad \text{and} \qquad u_\theta = -\frac{1}{r \sin\theta} \frac{\partial \psi}{\partial r} \tag{12}$$

The streamfunction for creeping flow in a spherical polar co-ordinate reference frame satisfies the following equation:

$$E^4(\psi) = E^2(E^2\psi) = 0 \qquad \text{where} \qquad E^2 = \frac{\partial^2}{\partial r^2} + \frac{\sin\theta}{r^2} \frac{\partial}{\partial \theta}\left(\frac{1}{\sin\theta} \frac{\partial}{\partial \theta} \right) \tag{13}$$

as detailed by Lamb [16], Richardson [17] or Ockendon *et al*. [18]. Note that in the case of spherical co-ordinates, E^2 does not equal ∇^2.

Equation 13 is a fourth-order partial differential operator on ψ and therefore requires four boundary conditions for its solution. The boundary conditions are determined by considering the constraints on the velocity field:

Zero normal flow on the surface of the sphere:

$$u_r = 0 \qquad \text{at} \qquad r = a \ , \ 0 \le \theta \le \pi \tag{14}$$

Slip flow around the surface of the sphere:

To account for non-continuum flow effects around the microsphere, the Navier-Stokes equations are solved in conjunction with the slip-velocity boundary condition proposed by Basset [15]:

$$\tau_t = \beta u_t \tag{15}$$

where u_t is the tangential slip velocity at the wall, τ_t is the tangential shear stress on the wall and β is the slip coefficient. Schaaf & Chambre [19] show that the slip coefficient can be related to the mean free path of the molecules as follows:

$$\beta = \frac{\mu}{\left(\frac{2-\sigma}{\sigma}\right)\lambda} \tag{16}$$

where μ is the viscosity of the gas, σ is the tangential momentum accommodation coefficient (TMAC) and λ is the mean free path. For an idealised wall (perfectly smooth at the molecular level), the angles of incidence and reflection of molecules colliding with the wall are identical and therefore the molecules conserve their tangential momentum. This is referred to as *specular reflection* and results in perfect slip at the boundary. Conversely, in the case of an extremely rough wall, the molecules are reflected at a totally random angle and lose their tangential momentum entirely; referred to as *diffusive reflection*. For real walls, some of the molecules will reflect diffusively and some will reflect specularly, and so the tangential momentum accommodation coefficient, σ, is introduced to account for the momentum retained by the reflected molecules. Theoretically, the coefficient lies between 0 and 1 and is defined as the fraction of molecules reflected diffusively. The value of σ depends upon the particular solid and gas involved and also on the surface finish of the wall. TMAC values lying in the range 0.2-1.0 have been determined experimentally by Thomas & Lord [20] and Arkilic *et al*. [21].

Equations (15) and (16) can be combined and rearranged to give

$$u_t = \frac{2-\sigma}{\sigma}\frac{\lambda}{\mu}\tau_t \tag{17}$$

which can be recast in terms of the Knudsen number, *Kn* as follows:

$$u_t = \frac{2-\sigma}{\sigma}\frac{Kn\,a}{\mu}\tau_t \tag{18}$$

where *Kn* is defined as the ratio of the mean free path of the molecules (λ) to the radius of the sphere:

$$Kn = \frac{\lambda}{a} \tag{19}$$

In the present analysis, the tangential shear stress on the surface of the sphere is denoted as $\tau_{r\theta}$ and the tangential velocity is simply u_θ. Consequently, the slip flow boundary condition (18) can be rewritten as

$$u_\theta = \frac{2-\sigma}{\sigma}\frac{Kn\,a}{\mu}\tau_{r\theta} \qquad at \quad r = a \;,\; 0 \le \theta \le \pi \tag{20}$$

Flow conditions at infinity:

As $r \to \infty$, the flow becomes a uniform stream of velocity U_∞ in the $\theta = 0$ direction which implies that

$$u_r = U_\infty \cos\theta \tag{21}$$

and

$$u_\theta = -U_\infty \sin\theta \tag{22}$$

Equation (22) can therefore be integrated to evaluate the streamfunction distribution as $r \to \infty$:

$$\psi = \int U_\infty \, r \sin^2\theta \, dr \tag{23}$$

giving

$$\psi(r \to \infty, \theta) = \frac{1}{2} U_\infty \, r^2 \sin^2\theta \tag{24}$$

Hence, $\psi(\theta) \propto \sin^2\theta$, but $\psi(r)$ is not as straight forward as $\psi(r) \propto r^2$ due to the velocity constraints on the surface of the sphere. The boundary conditions are prescribed at particular values of r (with θ being arbitrary), and therefore separating the variables leads to a solution of eqn. (13) in the form:

$$\psi(r, \theta) = f(r) \sin^2\theta \tag{25}$$

Substituting eqn. (25) into (13) gives

$$E^4(\psi) = E^2(E^2(\psi)) = \sin^2\theta \left(\frac{d^4}{dr^4} - \frac{4}{r^2}\frac{d^2}{dr^2} + \frac{8}{r^3}\frac{d}{dr} - \frac{8}{r^4} \right) f = 0 \tag{26}$$

or

$$\left(\frac{d^4}{dr^4} - \frac{4}{r^2}\frac{d^2}{dr^2} + \frac{8}{r^3}\frac{d}{dr} - \frac{8}{r^4} \right) f = 0 \tag{27}$$

Equation (27) is a linear, fourth-order ordinary differential equation. We assume a solution exists in the form:

$$f = C_n \, r^n \tag{28}$$

where C_n is a constant. Repeated differentiation of eqn. (28) yields

$$\left.\begin{aligned} f' &= C_n \, n \, r^{n-1} \\ f'' &= C_n \, n \, (n-1) \, r^{n-2} \\ f''' &= C_n \, n \, (n-1) \, (n-2) \, r^{n-3} \\ f'''' &= C_n \, n \, (n-1) \, (n-2) \, (n-3) \, r^{n-4} \end{aligned}\right\} \tag{29}$$

and substituting the derivatives shown in (29) into equation (27) gives

$$C_n\, r^{n-4}\left[n(n-1)(n-2)(n-3)-4n(n-1)+8n-8\right]=0 \tag{30}$$

which can be simplified to

$$C_n\, r^{n-4}\,(n+1)(n-1)(n-2)(n-4)=0 \tag{31}$$

Consequently the only possible solutions for *n* are

$$n=-1\,,1\,,2 \text{ or } 4 \tag{32}$$

Thus the general solution of eqn. (27) takes the form

$$f(r)=\frac{A}{r}+Br+Cr^2+Dr^4 \tag{33}$$

where *A*, *B*, *C* and *D* are constants. The streamfunction for creeping flow past a sphere therefore takes the form

$$\psi(r,\theta)=\left(\frac{A}{r}+Br+Cr^2+Dr^4\right)\sin^2\theta \tag{34}$$

Comparing eqn. (34) with the boundary condition shown in (24) reveals that *D* must be zero. If $D\neq 0$, then in the limit as $r\to\infty$, the streamfunction would vary according to r^4 and would contravene the r^2 variation implied in eqn. (24). Thus it follows that

$$C=\frac{1}{2}U_\infty \qquad \text{and} \qquad D=0 \tag{35}$$

Substituting eqn. (34) into (12) yields

$$u_r=\frac{1}{r^2\sin\theta}\left(\frac{A}{r}+Br+Cr^2+Dr^4\right)2\sin\theta\cos\theta \tag{36}$$

and

$$u_\theta=-\frac{1}{r\sin\theta}\left(-\frac{A}{r^2}+B+2Cr+4Dr^3\right)\sin^2\theta \tag{37}$$

Inserting the values evaluated in (35) into the above expressions therefore leads to

$$u_r=2\left(\frac{A}{r^3}+\frac{B}{r}+\frac{1}{2}U_\infty\right)\cos\theta \tag{38}$$

and

$$u_\theta=-\left(-\frac{A}{r^3}+\frac{B}{r}+U_\infty\right)\sin\theta \tag{39}$$

Prescribing the zero normal flow condition detailed in eqn. (14) results in

$$\frac{A}{a^3}+\frac{B}{a}+\frac{1}{2}U_\infty = 0 \tag{40}$$

For no-slip flows, as in the case of Stokes' original solution, the coefficients *A* and *B* are readily determined from (39) with $u_\theta = 0$ at $r = a$. However, in the present analysis, a second expression relating *A* and *B* is found using the slip-flow constraint of eqn. (20). In spherical co-ordinates, the shear stress acting on the "$r = \text{constant}$" plane in the θ-direction can be found from

$$\tau_{r\theta} = \mu\left(\frac{1}{r}\frac{\partial u_r}{\partial\theta}-\frac{1}{r}u_\theta+\frac{\partial u_\theta}{\partial r}\right) \tag{41}$$

But on the surface of the sphere

$$\frac{\partial u_r}{\partial\theta} = 0 \tag{42}$$

Substituting eqns. (41) and (42) into the slip-flow boundary condition (20) gives

$$u_\theta\big|_{r=a} = \frac{2-\sigma}{\sigma} Kn\, a\left(\frac{\partial u_\theta}{\partial r}-\frac{1}{r}u_\theta\right)\Bigg|_{r=a} \tag{43}$$

It is convenient at this stage to define

$$Kn' = \frac{2-\sigma}{\sigma} Kn \tag{44}$$

to simplify the resulting equations. Thus, eqn. (43) becomes

$$u_\theta\big|_{r=a} = Kn'\, a\left(\frac{\partial u_\theta}{\partial r}-\frac{1}{r}u_\theta\right)\Bigg|_{r=a} \tag{45}$$

which can be rearranged to give

$$u_\theta\big|_{r=a} = \frac{Kn'}{1+Kn'}\, a\,\frac{\partial u_\theta}{\partial r}\Bigg|_{r=a} \tag{46}$$

Differentiating eqn. (39) with respect to *r* yields

$$\frac{\partial u_\theta}{\partial r} = -\left(\frac{3A}{r^4}-\frac{B}{r^2}\right)\sin\theta \tag{47}$$

and substituting the result into eqn. (46) gives

$$u_\theta\big|_{r=a} = -\frac{Kn'}{1+Kn'}\left(\frac{3A}{a^3}-\frac{B}{a}\right)\sin\theta \tag{48}$$

Additionally, the tangential velocity on the surface of the sphere can be determined from eqn. (39):

$$u_\theta\big|_{r=a} = -\left(-\frac{A}{a^3}+\frac{B}{a}+U_\infty\right)\sin\theta \tag{49}$$

Equating (48) and (49) gives

$$-\frac{A}{a^3}+\frac{B}{a}+U_\infty = \frac{Kn'}{1+Kn'}\left(\frac{3A}{a^3}-\frac{B}{a}\right) \tag{50}$$

Solving for A and B from (40) and (50) finally yields

$$A = \frac{1}{4}U_\infty a^3\left(\frac{1}{1+3Kn'}\right) \quad \text{and} \quad B = -\frac{3}{4}U_\infty a\left(\frac{1+2Kn'}{1+3Kn'}\right) \tag{51}$$

As an aside, allowing $Kn' \to 0$ (continuum flow) results in the familiar values obtained in Stokes' solution:

$$A = \frac{1}{4}U_\infty a^3 \quad \text{and} \quad B = -\frac{3}{4}U_\infty a \tag{52}$$

4 Determination of the drag on the microsphere

The drag on the microsphere is composed of three separate components, namely skin-friction drag, normal stress drag and pressure (or form) drag.

4.1 *Drag due to skin-friction*

In spherical co-ordinates, the shear stress acting on the "$r = \text{constant}$" plane in the θ-direction can be found from

$$\tau_{r\theta} = \mu\left(\frac{1}{r}\frac{\partial u_r}{\partial\theta}-\frac{1}{r}u_\theta+\frac{\partial u_\theta}{\partial r}\right) \tag{53}$$

But on the surface of the sphere

$$\frac{\partial u_r}{\partial\theta} = 0 \tag{54}$$

Substituting eqns. (47), (49) and (54) into (53) and taking $r = a$ gives the shear stress distribution on the surface:

$$\tau_{r\theta}\big|_{r=a} = -6\mu \sin\theta \frac{A}{a^4} \tag{55}$$

The drag experienced by the sphere can then be found by resolving the shear stress in the direction of the incident free stream velocity and integrating the stress distribution around the entire surface, *S*. Specifically,

$$\text{Drag} = \iint -\tau_{r\theta}\big|_{r=a} \sin\theta \, dS \tag{56}$$

Consider a surface element composed of $\theta = \text{constant}$ and $\alpha = \text{constant}$ lines subtending angles of $d\theta$ and $d\alpha$. The surface area of the element, dS , is given by

$$dS = r^2 \sin\theta \, d\alpha \, d\theta \tag{57}$$

Therefore the drag can be rewritten as

$$\text{Drag} = a^2 \int_0^{2\pi} d\alpha \int_0^{\pi} -\tau_{r\theta}\big|_{r=a} \sin^2\theta \, d\theta \tag{58}$$

Inserting the shear stress from eqn. (55) leads to

$$\text{Drag} = \frac{12\pi\mu A}{a^2} \int_0^{\pi} \sin^3\theta \, d\theta = \frac{16\pi\mu A}{a^2} \tag{59}$$

and substituting for A from eqn. (51) yields

$$\text{Drag} = 4\pi\mu U_\infty a \left(\frac{1}{1+3Kn'} \right) \tag{60}$$

4.2 *Drag due to normal stress*

The shear stress acting on the "$r = \text{constant}$" plane in the *r*-direction is given by

$$\tau_{rr} = 2\mu \frac{\partial u_r}{\partial r} \tag{61}$$

In the case of continuum flows ($Kn \to 0$), it can be shown that the normal stress component is zero on the surface of the sphere and consequently the drag must also be zero. However, in the present analysis, the slip velocity boundary condition generates an additional drag component.

Differentiating eqn. (38) with respect to *r* and letting $r = a$ gives

$$\left.\frac{\partial u_r}{\partial r}\right|_{r=a} = 2\left(-\frac{3A}{a^4}-\frac{B}{a^2}\right)\cos\theta \tag{62}$$

and therefore the normal stress on the sphere is found to be

$$\tau_{rr}\big|_{r=a} = -4\,\mu\cos\theta\left(\frac{3A}{a^4}+\frac{B}{a^2}\right) \tag{63}$$

Again the drag is obtained by integrating the stress distribution around the surface of the sphere, giving

$$\text{Drag} = a^2\int_0^{2\pi} d\alpha \int_0^{\pi} \tau_{rr}\big|_{r=a}\sin\theta\cos\theta\, d\theta \tag{64}$$

Substituting the normal stress from eqn. (63) into (64) yields

$$\text{Drag} = -8\pi\mu\left(\frac{3A}{a^2}+B\right)\int_0^{\pi}\sin\theta\cos^2\theta\, d\theta = -\frac{16}{3}\pi\mu\left(\frac{3A}{a^2}+B\right) \tag{65}$$

and inserting the values of A and B from eqn. (51) then gives the drag due to the normal stress as follows:

$$\text{Drag} = 4\pi\mu U_\infty a\left(\frac{2Kn'}{1+3Kn'}\right) \tag{66}$$

It should be noted that substitution of the continuum flow solution ($Kn' = 0$) into the above equation results in zero drag, as expected.

4.3 *Drag due to pressure distribution*

The pressure distribution on the sphere is found by integrating *Stokes' equation* (7) using the velocity components defined in eqns. (38) and (39). Integration from a point at infinity where the pressure is p_∞ to a point at radius, r leads to

$$p = p_\infty + 2\mu\cos\theta\frac{B}{r^2} \tag{67}$$

Substituting for B from eqn. (51) then yields

$$p = p_\infty - \frac{3\mu\cos\theta U_\infty a}{2r^2}\left(\frac{1+2Kn'}{1+3Kn'}\right) \tag{68}$$

Integrating the pressure distribution around the surface of the sphere and noting that

the force on an elemental section of the surface due to the pressure is directed *inwards* towards the centre of the sphere gives

$$\text{Drag} = a^2 \int_0^{2\pi} d\alpha \int_0^{\pi} -p\big|_{r=a} \sin\theta \cos\theta \, d\theta \tag{69}$$

Substituting eqn. (68) into (69) and cancelling the term involving p_∞ which is constant and does not contribute to the drag leads to

$$\text{Drag} = 3\pi\mu U_\infty a \left(\frac{1+2Kn'}{1+3Kn'} \right) \int_0^{\pi} \sin\theta \cos^2\theta \, d\theta \tag{70}$$

Hence the drag due to the pressure distribution (the so-called "form-drag") is given by

$$\text{Drag} = 2\pi\mu U_\infty a \left(\frac{1+2Kn'}{1+3Kn'} \right) \tag{71}$$

4.4 *Summary of drag formulae*

The previous sections have detailed the individual drag components acting on the microsphere. The total drag experienced by the sphere is then found by summing these separate components. First, we recall the three drag components:

$$\text{Skin-friction drag} = 4\pi\mu U_\infty a \left(\frac{1}{1+3Kn'} \right) \tag{72}$$

$$\text{Normal stress drag} = 4\pi\mu U_\infty a \left(\frac{2Kn'}{1+3Kn'} \right) \tag{73}$$

$$\text{Form drag} = 2\pi\mu U_\infty a \left(\frac{1+2Kn'}{1+3Kn'} \right) \tag{74}$$

Summing the components gives

$$\text{Total drag} = 4\pi\mu U_\infty a \left(\frac{1+2Kn' + \frac{1}{2}(1+2Kn')}{1+3Kn'} \right) \tag{75}$$

which can be rewritten as

$$\text{Total drag} = 6\pi\mu U_\infty a\left(\frac{1+2Kn'}{1+3Kn'}\right) \tag{76}$$

It can be seen that the total drag on the sphere is composed of Stokes' drag law ($6\pi\mu U_\infty a$) for continuum flows multiplied by a rarefaction coefficient dependent upon the Knudsen number:

$$\left(\frac{1+2Kn'}{1+3Kn'}\right) \tag{77}$$

Writing the above rarefaction coefficient in terms of the true Knudsen number then gives the total drag expression as

$$\text{Total drag} = 6\pi\mu U_\infty a\left(\frac{1+2\dfrac{2-\sigma}{\sigma}Kn}{1+3\dfrac{2-\sigma}{\sigma}Kn}\right) \tag{78}$$

5 Application of slip flow past a sphere - correction for the terminal velocity of a free-falling microsphere

One of the most practical applications of slip flow past a sphere is the determination of the terminal velocities of minute particles settling in a gas. When the diameter of the particles approaches the mean free path of the gas molecules, it is important to account for non-continuum flow effects. The analysis is best exemplified by Millikan's oil drop experiment for the measurement of the charge of an electron [22,23]. Millikan employed oil drops having a radius of the order of 10^{-6} m and measured the mass of the drops by observing their terminal velocities. He was aware of the limitation of Stokes' Law as the size of the oil drops diminished, and proposed an empirical first-order correction technique to allow for rarefaction effects. The present analytical solution allows us to revisit Millikan's approach and demonstrate the applicability of the slip-flow analysis.

Consider a spherical oil drop of radius, a and density, ρ_{oil} settling at a terminal velocity, U in air of density, ρ_{air}. Equating the downwards gravitational force on the drop to the upwards buoyancy and drag forces, and utilising the analytical slip-flow correction given in eqn. (76) yields

$$\frac{4}{3}\pi a^3\rho_{oil}\, g = 6\pi\mu U\, a\left(\frac{1+2Kn'}{1+3Kn'}\right)+\frac{4}{3}\pi a^3\rho_{air}\, g \tag{79}$$

or

$$\frac{4}{3}\pi a^3(\rho_{oil}-\rho_{air})\,g = 6\pi\mu U\,a\left(\frac{1+2Kn'}{1+3Kn'}\right) \tag{80}$$

Rearranging for the terminal velocity then gives

$$U = \frac{2}{9}\frac{g\,a^2}{\mu}(\rho_{oil}-\rho_{air})\left(\frac{1+3Kn'}{1+2Kn'}\right) \tag{81}$$

and therefore the correction factor to be applied to the terminal velocity due to the Knudsen number can be expressed as

$$\left(\frac{1+3Kn'}{1+2Kn'}\right) \tag{82}$$

Without recourse to an analytical solution, Millikan realised that the increase in terminal velocity above the value predicted by Stokes' Law should be some function of λ / a : (the term Knudsen number was not used at the time). Millikan argued that the terminal velocity of the oil droplets should have the general form

$$U = \frac{2}{9}\frac{g\,a^2}{\mu}(\rho_{oil}-\rho_{air})\left(1+ f\left(\frac{\lambda}{a}\right)\right) \tag{83}$$

In the absence of further information, Millikan expressed the function, *f* as a power series:

$$f = A\left(\frac{\lambda}{a}\right)+B\left(\frac{\lambda}{a}\right)^2+C\left(\frac{\lambda}{a}\right)^3+... \tag{84}$$

where *A*, *B*, *C* etc. are constants. By assuming that the departure from Stokes' Law was small, Millikan neglected the second-order terms in eqn. (84) and therefore expressed the terminal velocity as

$$U = \frac{2}{9}\frac{g\,a^2}{\mu}(\rho_{oil}-\rho_{air})\left(1+ A\left(\frac{\lambda}{a}\right)\right) \tag{85}$$

where *A* was a dimensionless constant which was found experimentally to be 0.874.

Ignoring the motion of the oil inside the drop and assuming a tangential momentum accommodation coefficient of unity allows a direct comparison of Millikan's results with the analytical correction factor given in eqn. (82). Figure 2 compares the velocity correction factors and shows that the present analytical method and Millikan's experimentally determined correction are in good agreement over the lower range of Knudsen numbers ($Kn \le 0.1$). For higher Knudsen numbers, the slip-flow extension of the Navier-Stokes equations is no longer justifiable since the Navier-Stokes equations are only first-order accurate in Knudsen number [6]. However, Millikan's linearised correction technique cannot be justified for large *Kn*

either. The agreement between the experimental and theoretical predictions at lower Knudsen numbers therefore confirms the applicability of the slip-flow analysis.

6 Numerical validation

The proposed analytical solution is ideal for validating numerical models operating in the slip-flow regime ($Kn \leq 0.1$). In the present study, the analytical drag formulae have been used to validate a slip-flow extension of the boundary-fitted Navier-Stokes solver developed by the Computational Engineering Group at CLRC Daresbury Laboratory [24]. Instead of considering an unconfined flow geometry, the numerical simulations employed a sphere inside a circular pipe as illustrated schematically in Figure 3. This geometry is commonly utilised in macro-scale spinning rotor gauge devices for the determination of pressure, viscosity or molecular weights in low pressure gases [25,26]. The problem has also been studied numerically over a wide range of Knudsen numbers by Liu *et al*. [27]. Simulating different blockage ratios (H / D) allows an assessment to be made of the asymptotic approach to the unconfined flow situation. In the present study, blockage ratios between 2:1 and 40:1 were considered. The problem was simplified by assuming that the flow was axisymmetric and incompressible (low Mach number). Numerical tests accounting for compressibility showed very little difference in the flow solution and therefore justified the low Mach number simplification.

A parabolic slip-flow profile was prescribed at the inflow of the computational domain and the upstream and downstream boundaries were located sufficiently far away from the sphere so as to not to affect the flow solution. The drag components on the sphere were computed using numerical integration of the stress distributions. Rarefaction effects were included in the Navier-Stokes solver using the slip-flow boundary condition presented earlier:

$$u_t = \frac{2-\sigma}{\sigma} \frac{Kn\, a}{\mu} \tau_t \tag{86}$$

The model was run at various Reynolds numbers less than 1.0 and all simulations showed remarkably similar normalised drag components. The results presented here utilise a Reynolds number, *Re*, of 0.125 where

$$Re = \frac{\rho \bar{U}\, a}{\mu} \tag{87}$$

and $\bar{U}$ is the mean velocity inside the pipe.

Figure 4 presents the variations in the computed drag components on the sphere as a function of Knudsen number for the widest blockage ratio considered (40:1). The drag components have been normalised with respect to Stokes' Law ($6\pi\mu U_\infty a$) so as to allow a direct comparison against the continuum flow solution. It should be noted that the analytical drag results presented in Figure 4 have been computed by multiplying the unconfined flow equations by a factor of two to account for the fact

that the velocity at the centre of the pipe is twice the mean value. Figure 4 shows very good agreement between the numerical and analytical solutions over the range of Knudsen numbers considered. Small discrepancies can be seen in the numerical predictions of the drag due to the normal stress, but these are thought to be caused by inadequacies in the mesh close to the sphere. This can be confirmed by noting that the numerical model fails to predict a normal stress drag component of zero in the continuum flow regime ($Kn \to 0$). The numerical model predicts slightly larger drag forces than the analytical solution but this is to be expected since the sphere is still experiencing a slight blockage effect within the pipe. Nevertheless, the general agreement between the predictions appears to confirm the validity of the numerical solution.

7 Conclusions

An extension of Stokes' analytical solution for creeping flow past a sphere has been derived which accounts for rarefaction (non-continuum) effects in gases. The analysis has shown that the total drag experienced by the sphere is equivalent to Stokes' solution for continuum flows multiplied by a rarefaction coefficient dependent upon the Knudsen number. The analysis is applicable to the *slip-flow* regime and is valid for Knudsen numbers less than 0.1.

The analytical drag formulae have been validated against experimental results from Millikan's oil drop experiment. When the size of an oil drop approaches the mean free path of the gas molecules, rarefaction effects increase the terminal velocity above that predicted by Stokes' continuum solution. The present slip-flow analysis yields very good agreement with the empirical drag correction technique proposed by Millikan.

The analytical solution for the total drag contains three contributing components: pressure drag, skin-friction drag and normal stress drag. These components can be used to validate CFD codes that have been extended to model gaseous transport in micro-scale geometries. For the flows under consideration, a finite-volume Navier-Stokes solver has been modified to account for the slip-boundary conditions found at solid walls. Close agreement between the analytical and numerical results has been demonstrated and confirms both the validity of the numerical code and the benefit of the analytical slip-flow solution.

References

[1] Gabriel, K., Jarvis, J. & Trimmer, W. (eds.) *Small Machines, Large Opportunities: a report on the emerging field of microdynamics*, National Science Foundation, AT&T Bell Laboratories, Murray Hill , New Jersey, USA, 1988.

[2] Gravesen, P., Branebjerg, J. & Jenson, O.S. Microfluidics – a review, *J. Micromechanics and Microengineering*, Vol. 3, pp. 168-182, 1993.

[3] Gad-el-Hak, M. The fluid mechanics of microdevices – The Freeman scholar lecture, *J. of Fluids Engineering*, Vol. 121, pp. 5-33, 1999.

[4] Beskok, A. & Karniadakis, G.E. Simulation of heat and momentum transfer in complex microgeometries, *J. Thermophysics and Heat Transfer*, Vol. 8, No. 4, 1994.

[5] Beskok, A., Karniadakis, G.E. & Trimmer, W. Rarefaction, compressibility and thermal creep effects in micro-flows, *Proc. of the ASME Dynamic Systems and Control Division*, pp. 877-892, ASME, 1995.

[6] Beskok, A. *Simulations and models for gas flows in microgeometries*, Ph.D. Thesis, Princeton University, Princeton, New Jersey, 1996.

[7] Pfahler, J., Harley, J., Bau, H. & Zemel, J.N. Gas and liquid flow in small channels, DSC-Vol. 32, *Micromechanical Sensors, Actuators and Systems*, pp. 49-60, ASME, 1991.

[8] Harley, J.C., Huang, Y., Bau, H.H. & Zemel, J.N. Gas flow in microchannels, *J. Fluid Mech.*, Vol. 284, pp. 257-274, 1995.

[9] Arkilic, E.B. & Breuer, K.S. Gaseous flow in small channels, *AIAA Shear Flow Conference*, Paper no. AIAA 93-3270, Orlando, 1993.

[10] Arkilic, E.B., Breuer, K.S. & Schmidt, M.A. Gaseous flow in microchannels, FED-Vol. 197, *Application of Microfabrication to Fluid Mechanics*, pp. 57-66, ASME, 1994.

[11] Arkilic, E.B., Schmidt, M.A. & Breuer, K.S. Gaseous slip flow in long microchannels, *J. of Micro-Electro-Mechanical Systems*, Vol. 6, No. 2, pp. 167-178, 1997.

[12] Arkilic, E.B. *Measurement of the mass flow and tangential momentum accommodation coefficient in silicon micromachined channels*, Ph.D. Thesis, Massachusetts Institute of Technology, Cambridge, Massachusetts, 1997.

[13] Fan, Q. & Xue, H. Compressible effects in microchannel flows, *Proc. 2nd IEEE/CPMT Electronics Packaging Technology Conference*, Piscataway, New Jersey, USA, pp. 224-228, 1998.

[14] Stokes, G.G. On the effect of the internal friction of fluids on the motion of pendulums, *Cambridge Phil. Trans.*, Vol. 9, pp. 8-106, 1851.

[15] Basset, A.B. *Hydrodynamics*, Deighton, Bell & Co., Cambridge, 1888.

[16] Lamb, H. *Hydrodynamics*, Cambridge University Press, 6th Ed., 1952.

[17] Richardson, S.M. *Fluid Mechanics*, Hemisphere Publishing Corp., 1989.

[18] Ockendon, H. & Ockendon, J.R. *Viscous Flow*, Cambridge University Press, 1995.

[19] Schaaf, S.A. & Chambre, P.L. *Flow of Rarefied Gases*, Princeton University Press, 1961.

[20] Thomas, L.B. & Lord, R.G. Comparative measurements of tangential momentum and thermal accommodations on polished and on roughened steel spheres, *Rarefied Gas Dynamics* 8, pp. 405-412, ed. K. Karamcheti, Academic Press, New York, 1974.

[21] Arkilic, E.B., Schmidt, M.A. & Breuer, K.S. TMAC measurement in silicon micromachined channels, *Rarefied Gas Dynamics 20*, Beijing University Press, 1997.
[22] Millikan, R.A. The general law of fall of a small spherical body through a gas, and its bearing upon the nature of molecular reflection from surfaces, *Physical Review*, 22(1), pp. 1-23, 1923.
[23] Millikan, R.A. *The Electron: its isolation and measurement and the determination of some of its properties*, University of Chicago Press, 8th Ed., 1963.
[24] Gu X.J. & Emerson, D.R. *THOR-2D: A two-dimensional computational fluid dynamics code*, Technical Report, Department of Computational Science and Engineering, CLRC Daresbury Laboratory, June 2000.
[25] Fremerey, J.K. Spinning rotor vacuum gauges, *Vacuum*, Vol. 32, pp. 685-690, 1982.
[26] Reich, G. Spinning rotor viscosity gauge: A transfer standard for the laboratory or an accurate gauge for vacuum process control, *J. Vacuum Science and Technology*, Vol. 20(4), pp. 1148-1152, 1982.
[27] Liu, H-C. F., Beskok, A., Gatsonis, N. & Karniadakis, G.E. Flow past a micro-sphere in a pipe: effects of rarefaction, DSC-Vol. 66, *Micro-Electro-Mechanical Systems (MEMS)*, pp. 445-452, ASME, 1998.
[28] *CRC Handbook of Chemistry and Physics*, 80th Ed., CRC Press, 1999-2000.

Appendix

For an ideal gas modelled as rigid spheres of diameter, σ, the mean distance travelled by a molecule between successive collisions or *mean free path*, λ, is given by [28]:

$$\lambda = \frac{kT}{\sqrt{2}\,\pi\, p\,\sigma^2} \tag{1}$$

where,

k = Boltzmann's constant = 1.380662×10^{-23} J / K,

T = temperature (K),

p = pressure (N/m^2) and

σ = collision diameter of the molecules (m).

At standard ambient conditions ($p = 10^5$ N/m^2 and T = 298.15 K), the expression becomes:

$$\lambda = \frac{9.265\times10^{-27}}{\sigma^2} \tag{2}$$

For air, the average collision diameter of the molecules is 3.66×10^{-10} m giving a mean free path of 6.92×10^{-8} m (or 69.2 nm).

The table below details the collision diameters of other common gases.

Gas	σ (m)
Air	3.66×10^{-10}
Ar	3.58×10^{-10}
CO_2	4.53×10^{-10}
H_2	2.71×10^{-10}
He	2.15×10^{-10}
Kr	4.08×10^{-10}
N_2	3.70×10^{-10}
NH_3	4.32×10^{-10}
Ne	2.54×10^{-10}
O_2	3.55×10^{-10}
Xe	4.78×10^{-10}

Table A1: Collision diameters of common gases [28]

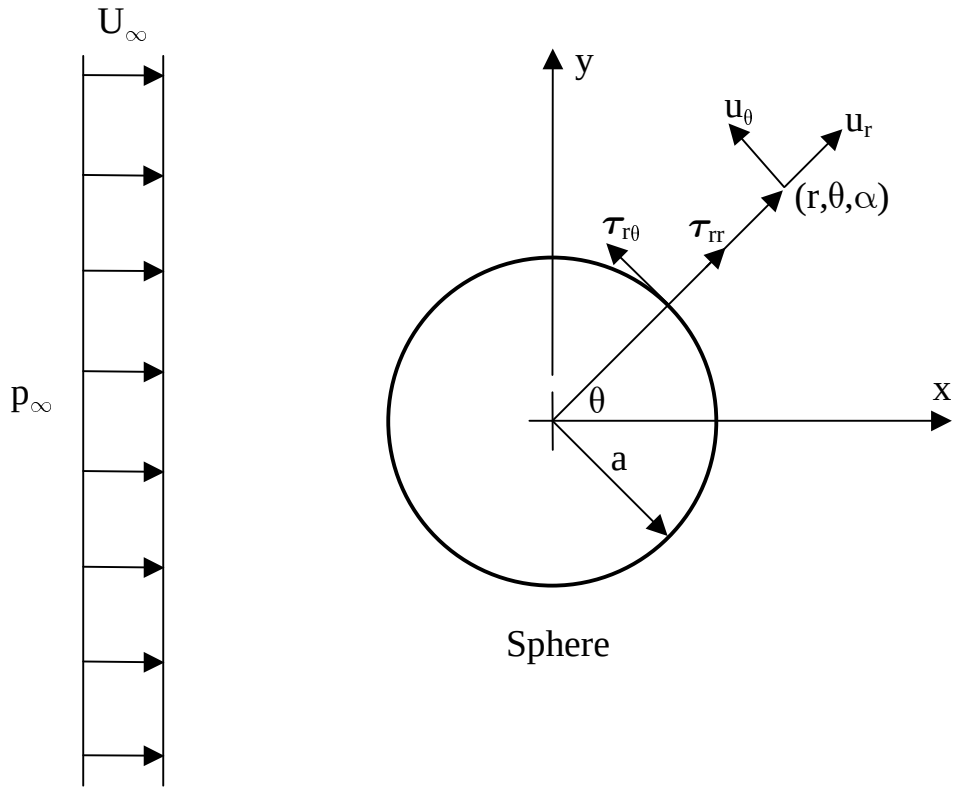

Figure 1: Problem formulation

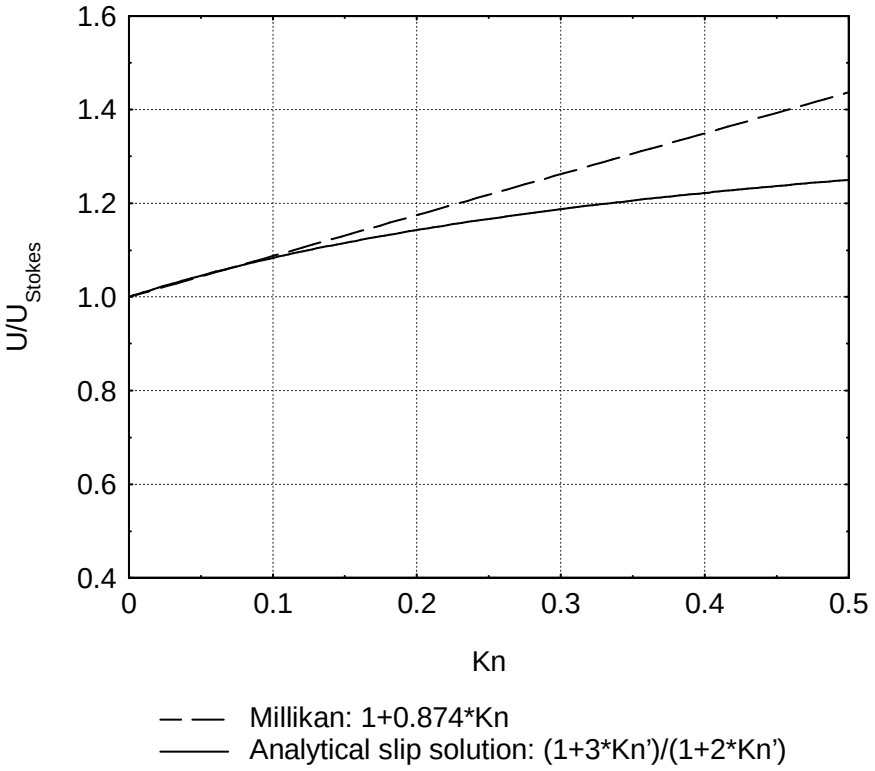

Figure 2: Variation of terminal velocity of oil drops as a function of Knudsen number (Kn)

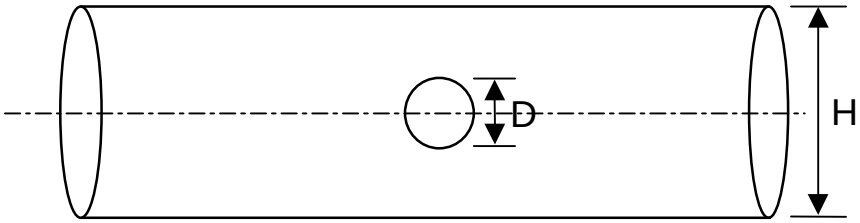

(a) Flow geometry

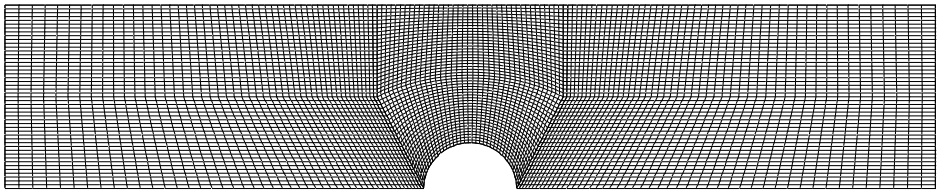

(b) Axisymmetric flow domain for $H/D = 4$

Figure 3: Confined flow past a sphere in a circular pipe

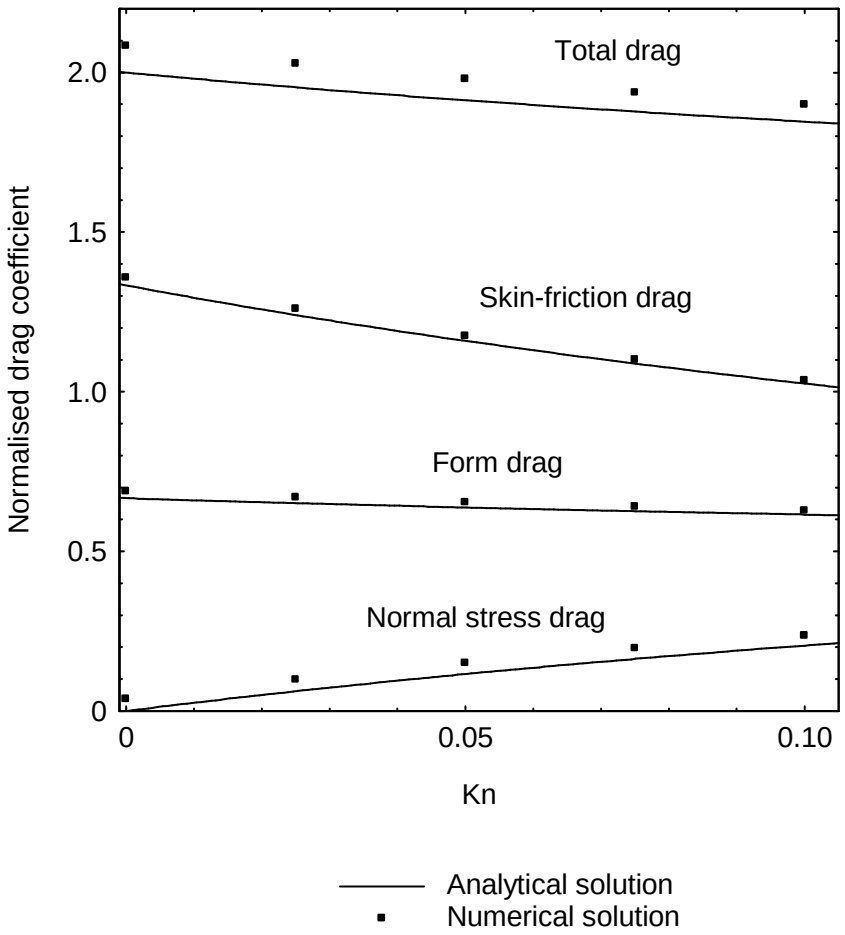

Figure 4: Variation of drag components as a function of Knudsen number (Kn) for a blockage ratio of $H/D = 40$